

RSC Advances



This is an *Accepted Manuscript*, which has been through the Royal Society of Chemistry peer review process and has been accepted for publication.

Accepted Manuscripts are published online shortly after acceptance, before technical editing, formatting and proof reading. Using this free service, authors can make their results available to the community, in citable form, before we publish the edited article. This *Accepted Manuscript* will be replaced by the edited, formatted and paginated article as soon as this is available.

You can find more information about *Accepted Manuscripts* in the [Information for Authors](#).

Please note that technical editing may introduce minor changes to the text and/or graphics, which may alter content. The journal's standard [Terms & Conditions](#) and the [Ethical guidelines](#) still apply. In no event shall the Royal Society of Chemistry be held responsible for any errors or omissions in this *Accepted Manuscript* or any consequences arising from the use of any information it contains.

ARTICLE

Cite this: DOI: 10.1039/x0xx00000x
Controlled Synthesis of High Metal Loading Pt based Electrocatalysts with Enhanced Activity and Durability toward Oxygen Reduction ReactionShushuang Li,^a Huiyuan Liu,^a Ying Wang,^{a,b} Wei Xu,^{a,b} Jia Li,^{a,b} Yuan Liu,^a Xinwen Guo,^b and Yujiang Song^{*a}Received 00th January 2012,
Accepted 00th January 2012

DOI: 10.1039/x0xx00000x

www.rsc.org/

High metal loading Pt/C electrocatalysts are highly desired for the fabrication of thin-layered membrane electrode assemblies (MEA) suitable for mass transport and balance control over water and heat. However, such electrocatalysts are still limited to commercial Pt/C comprised of carbon supported 2-5 nm Pt particles without size and size uniformity control, causing poor activity and durability toward oxygen reduction reaction (ORR). Herein, we report controlled synthesis of 59.9 wt% Pt/C by using metallic ion-containing reversed micelles adsorbed on carbon. Combined with a simple surfactant removal method by water washing, this unique confining approach enables an easy control over the size and size uniformity of the resultant Pt/C, leading to significantly improved activity and durability for ORR compared with commercial 60 wt% Pt/C. The ORR activity enhancement arises from a smaller average size of Pt nanoparticles in combination with a narrower size distribution, making more Pt nanoparticles falling in an optimal size range of 2-4 nm with the highest ORR activity. The narrower size distribution of our Pt/C also makes the Pt nanoparticles resistant to dissolution/re-deposition Ostwald ripening process in which small Pt nanoparticles gradually shrink until disappear while large ones get bigger and bigger.

Introduction

Owing to world-wide intensive studies on proton exchange membrane fuel cells (PEMFCs) during the past two decades this clean and efficient energy conversion technology is close to the pre-commercialization stage for automotive applications.¹ A crucial component of PEMFC is Pt/C electrocatalysts for ORR at the cathode side. However, the limited ORR activity and durability of Pt/C has become the main bottleneck, preventing PEMFC from widespread applications.²

In order to improve the ORR activity and durability of Pt/C, two strategies have been investigated. One promising yet long-run resolution is to replace noble metals with cheap and abundant counterparts while retaining or surpassing the overall performance of Pt/C. In this regard, significant progress on non-noble metal electrocatalysts has been made, especially for those applied in alkaline media.³ For example, Chung and Zelenay reported a novel nitrogen-doped carbon nanotube/nanoparticle composite ORR electrocatalyst obtained from pyrolysis of iron acetate as an iron precursor and cyanamide as a nitrogen and carbon nanotube precursor. When used at a sufficiently high loading, the composite outperforms commercial 20 wt% Pt/C at 60 $\mu\text{g}_{\text{Pt}}/\text{cm}^2$ in an alkaline solution.^{3a} Dai and his co-workers designed a class of 2D

covalent organic polymers with precisely controlled locations of nitrogen heteroatoms and pore sizes, followed by complexation with metal and carbonization of the metal-incorporated materials, which exhibited a similar onset potential as that of the Pt/C both with a loading of 0.2 mg cm^{-2} .^{3f} The other near-term and more realistic resolution is to develop novel platinum based electrocatalysts,⁴ like PtCo/C,⁵ PtNi/C,⁶ PtAu/C,⁷ and so on.⁸ Recently, Yang and Stamenkovic created an intriguing Pt₃Ni nanoframe electrocatalyst by leaching out nickel from platinum-nickel bimetallic nanocrystals. Compared with commercial Pt/C, this nanoframe electrocatalyst remarkably achieved a factor of 36 enhancement in mass activity and a factor of 22 enhancement in specific activity toward ORR.^{4a} Wang and Abruña reported ordered intermetallic platinum-cobalt core-shell nanoparticles with over 200% increase in ORR mass activity and over 300% increase in ORR specific activity relative to commercial Pt/C.⁵ Lou and his coworkers described a novel 3D Pt nanoassembly consisting of 1D single crystalline Pt nanowires with an excellent resistance to dissolution, migration, Ostwald ripening, and aggregation because of the 1D structural characteristics.^{8a} In particular, it is worth pointing out that high metal loading Pt/C electrocatalysts (around or over 50 wt%) allows the

fabrication of thin-layered MEA, which is highly desired for the sake of Pt utilization efficiency improvement and the balance control of water and heat.⁹ However, such electrocatalysts are still limited to commercial Pt/C comprised of carbon supported Pt particles without size and size uniformity control, causing poor activity and durability toward ORR.¹⁰

Herein, we report controlled synthesis of 59.9 wt% Pt/C by using metallic ion-containing reversed micelles adsorbed on carbon.¹¹ The key to the controlled synthesis is that the reduction of platinum complex is confined in the separate micellar interior localized on carbon, preventing individual platinum nanoparticles from growing into large ones and agglomeration. In addition, we developed a simple purification procedure to effectively remove the micelles by washing with hot water for multiple times while keeping platinum nanoparticles intact afterwards. This unique synthetic approach enables an easy control over the size and size uniformity of the resultant electrocatalysts at a high metal loading, leading to significantly improved activity and durability for ORR compared with commercial 60 wt% Pt/C. The improved ORR activity arises from a smaller average size of Pt nanoparticles supported on carbon in combination with a narrower size distribution. In this scenario, there are many more Pt nanoparticles falling in an optimal size range of 2-4 nm, which is well known to possess the highest ORR activity. The narrower size distribution of our Pt/C also makes the Pt nanoparticles resistant to dissolution/re-deposition Ostwald ripening process in which small Pt nanoparticles gradually shrink until disappear while large ones get bigger and bigger.¹² With a narrower size distribution, the size difference among individual Pt nanoparticles is relatively small, and thus the dissolution and re-deposition process of Pt evenly occurs upon each Pt nanoparticle, accordingly slowing down the Ostwald ripening process.

Experimental

Chemicals

Potassium tetrachloroplatinate (K_2PtCl_4 , 99 wt%), potassium chloropalladate (K_2PdCl_4 , 99 wt%), sodium tetrachloroaurate ($NaAuCl_4$, 99 wt%), potassium pentachlororuthenate (K_2RuCl_5 , 99 wt%), sodium hexachloroiridate (Na_2IrCl_6 , 99 wt%) were purchased from Fengchuan Chemical Reagent Co. (Tianjin, China), cetyltrimethylammonium bromide (CTAB, 99%) (Sigma-Aldrich), chloroform (Sinopharm Chemical Reagent), and sodium borohydride (Acros organics, 99%) were used as received. All aqueous solutions were prepared with ultrapure water (18.2 M Ω ·cm at 25 °C) produced from a Millipore water system (Synergy® UV, France). The stock solution of platinum(II) complexes (20 mM) was prepared by dissolving K_2PtCl_4 in water and allowing it to age for at least 24 h before use. Aging the stock solution disproportionates the complex into an equilibrium mixture of 42% $Pt(H_2O)_2Cl_2$, 53% $Pt(H_2O)Cl_3^-$, and 5% $PtCl_4^{2-}$.

Synthesis of Pt/C with different metal loading

Certain amount of VXC-72 or EC-600 carbon black was added to 10 mL of chloroform containing 40 mM CTAB with the aid of sonication. The suspension turned black and no black precipitates were observed, which suggested well dispersion of carbon black in chloroform. Then, 10 mL of 20 mM aged K_2PtCl_4 aqueous solution was mixed with the carbon-containing chloroform. The synthetic system was left under stirring under ambient conditions for 1 h to guarantee the complete transfer of the metallic complexes to the micelle-containing chloroform phase. The mixture was transferred to a 250 mL glass bottle, and 90 mL of nanopure water and 10 mL of 300 mM sodium borohydride was added under stirring at a speed of 1600 rpm. Bubbles were observed during the reaction process. Finally, we purified the electrocatalyst simply by washing with copious amount of water at 90-100 °C.

K_2PtCl_4 can be replaced by K_2PdCl_4 , $NaAuCl_4$, and K_3FeCl_6 , K_2CoCl_4 thus a variety of electrocatalysts can be synthesized, including PtPd/C, PtFe/C, PtCo/C, and Pt_3PdAu/C .

Instrumentation

TEM (JEOL JEM-2100, 200 KeV) was performed on obtained platinum nanomaterials. The samples for electron microscopy analysis were prepared by adding drops of colloidal suspensions onto a standard copper grid and wicking away the excess liquid with a filter paper. The grids were air-dried for at least 2 h before imaging. X-ray diffraction (XRD) spectra (PANalytical PW3040/60 X' Pert PRO) were recorded using Cu K α radiation source ($\lambda = 0.15432$ nm) in θ -2 θ scan mode at a scanning rate of 5° min⁻¹. Thermogravimetry (TG) analysis was performed (SDT Q600) with dried air as the processing atmosphere and a heating rate of 10 °C per minute. UV-visible spectra were obtained with a spectrophotometer (Analytic Jena, Specord S600) and a 0.2 cm path length quartz cell.

Electrochemical Measurements

An Autolab potentiostat/galvanostat (Echo Chemie BV Model PGSTAT-302N, Netherlands) was used for the electrochemical measurements in a conventional three-electrode electrochemical cell installed with platinum mesh as the counter electrode and a saturated calomel electrode (SCE) as the reference electrode that is connected to the cell by a salt bridge (agar gel containing saturated KNO_3). All potentials in this study were referred to reversible hydrogen electrode (RHE). All electrochemical measurements were performed at 25 °C.

Certain amount of water, ethanol, and Nafion solution (5 wt% Dupont) (1:9:0.06) was mixed with an electrocatalyst and sonicated in a water bath for 20 min to obtain catalyst ink (1 mg/mL). Glassy carbon rotating disk electrodes (RDE, 0.196 cm², Pine Instruments, USA) were polished with 0.05 μ m Bio-Analytical Systems (BAS) alumina paste and purged with N_2 prior to deposition of catalyst ink. The catalyst ink (10 μ L) was transferred onto the glassy carbon RDE and then evaporated the solvent in the air. The metal loading is 30.6 and 30.0 μ g_{Pt}cm⁻²

for commercial 60 wt% Pt/C and 59.9 wt% Pt/C, respectively. Potential cycling (100 mVs⁻¹) between 0 and 1.2 V was applied to the electrodes to obtain stable and repeatable cyclic voltammetry (CV) curves in N₂ purged aqueous HClO₄ (0.1 M). The electrochemically active surface area (ECSA) of the catalysts was determined by integrating the hydrogen desorption area between 50 and 460 mV of CV curves obtained at a scan rate of 50 mV s⁻¹ (assuming 210 μC cm_{Pt}⁻² for the desorption of a monolayer of hydrogen).

The ORR polarization curve of the catalysts was recorded using catalyst-coated RDE in O₂ saturated HClO₄ (0.1 M) aqueous solution with a positive sweep rate of 10 mVs⁻¹ at 1600 rpm. Current densities in the ORR polarization curves were normalized to the geometric area of the glassy carbon RDE. Mass activity (MA) and specific activity (SA) were determined based on ORR polarization curves.

For accelerated durability test (ADT), the same electrocatalyst-coated glassy carbon RDEs were used as the working electrode. The electrodes were cycled between 0.6 and 1.2 V for a total number of 2500 cycles in O₂ saturated HClO₄ (0.1 M). The scan rate was kept at 100 mVs⁻¹ during the process of potential cycling. Meanwhile, CV curves and ORR polarization curves were collected in aqueous HClO₄ solution (0.1 M) at certain cycles to track the degradation of electrocatalysts.

Results and Discussion

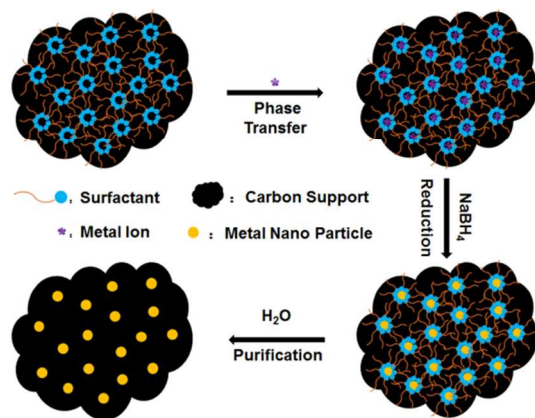


Figure 1. Schematic illustration of the synthesis and purification of electrocatalysts using metallic ion-containing reversed micelles adsorbed on carbon

In a typical synthesis, CTAB was dissolved in chloroform, forming reversed micelles via molecular self-assembly process that was investigated by us previously.¹³ Initially, carbon black powder (VXC-72 or EC-600) was added with the aid of mild sonication in a water bath to well disperse carbon and to ensure the adsorption of reversed micelles (Figure 1). Next, K₂PtCl₄ aqueous solution was placed in the mixture. The electrostatic interaction between positively charged CTA⁺ and negatively charged metallic complexes PtCl₄²⁻ drives metallic complexes to automatically transfer from aqueous phase to the interior of reversed micelles in chloroform. UV-visible spectrum of the

supernatant obtained after phase transfer (Figure S1) shows no characteristic peaks of Pt (II) complexes, verifying that the transfer of PtCl₄²⁻ is complete. In the following, NaBH₄ aq. was added in to reduce metallic complexes confined in the micellar interior. Lastly, the obtained electrocatalyst was simply purified by washing with copious amount of water at 90-100 °C.

To demonstrate the efficacy of this approach and for the significance of the high metal loading electrocatalyst, we carried out the synthesis of 60 wt% Pt/C electrocatalyst. After purification, the metal loading of the electrocatalyst was determined to be 59.9 wt% according to thermogravimetry analysis (TGA) as shown in Figure S2. Transmission electron microscopy (TEM) images reveal that all platinum nanostructures are well dispersed on carbon without free standing particles (Figure 2a), suggestive of the effective adsorption of reversed micelles and subsequent nucleation and growth of platinum on carbon. Platinum nanoparticles are evenly distributed on carbon without large agglomerations that apparently occurred in commercial 60 wt% Pt/C (Fig. 2d). The average diameter of the platinum nanoparticles of our 59.9 wt% Pt/C is 3.6 ± 0.7 nm with a size distribution of 20.4%. In contrast, commercial 60 wt% Pt/C has a relatively large average diameter of 4.4 ± 1.3 nm with a much wider size distribution of 29.9% (Fig. 2d). It is worth pointing out that the high surface area of carbon (EC-600, 1270 m²/g) is a prerequisite for the synthesis of Pt/C with a high metal loading. If the surface area of carbon is low, there would be no enough nucleation sites available for platinum, causing unsupported platinum nanoparticles.

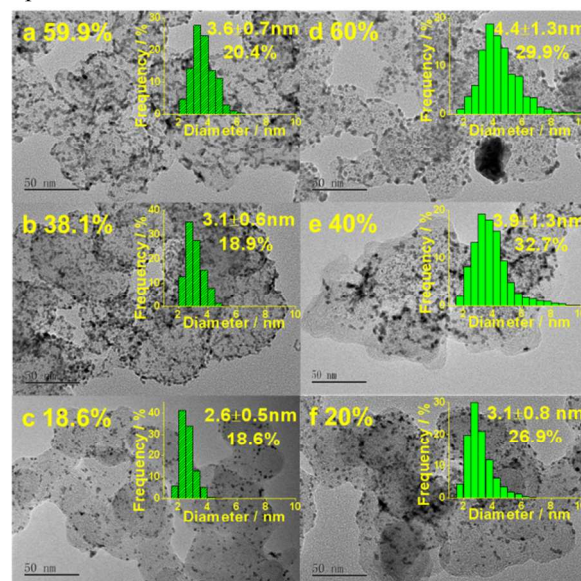


Figure 2. TEM images of Pt/C electrocatalyst synthesized by using metallic ions-containing micelles at different metal loadings: (a) 59.9 wt%, (b) 38.1 wt%, (c) 18.6 wt%; commercial Pt/C at similar metal loadings: (d) 60 wt%, (e) 40 wt%, and (f) 20 wt%. (Insets: Average diameters were measured for over 300 nanostructures, and their frequencies are plotted in the inset graphs. The average size and the standard deviations are given in the plots, along with the percentage ratio of the standard deviation to average size.)

By varying the ratio between platinum precursor and carbon, we can easily manipulate the metal loading of Pt/C electrocatalysts roughly from 20 to 60 wt% (Figure S2). As the metal loading decreases to 38.1 and 18.6 wt%, the average size of our Pt/C slightly changes to 3.1 ± 0.6 and 2.6 ± 0.5 nm, respectively. Meanwhile, the size distribution remains almost unchanged (18.9 % and 18.4) (Figure 2b-c), further verifying the successful control over the size distribution. In contrast, the average size of commercial 40 and 20 wt% Pt/C also decreases a little to 3.9 ± 1.3 and 3.1 ± 0.8 nm, respectively. However, the corresponding average size and size distribution turn to much larger than that of our Pt/C at a similar metal loading (Fig. 2e-f). This clearly shows the realization of the size and size uniformity control of our approach over the electrocatalysts at a wide range of metal loadings. This control is originating from the confining effect of reversed micelles.

To confirm the size control over Pt/C at varied metal loadings, the electrocatalysts were subject to XRD measurements (Figure S3). The broadened peak at 39.6° , 46.2° and 67.8° is originating from (111), (200), (220) diffraction of face centred cubic (fcc) platinum, respectively. Scherrer equation was used to calculate the average crystalline size based on full width at half maximum (FWHM) of (220) peak for each sample. As-determined crystalline size of our Pt/C increases from 2.3 to 2.7 to 2.8 nm with the increase of metal loading, analogous to the sizes determined by TEM. The overall size incremental is merely 0.5 nm, clearly exemplifying the successful size control due to micellar confining. In contrast, the size of commercial Pt/C changes from 2.5 to 3.3 to 3.8 nm as metal loading increases and the total size variation is 1.3 nm (Fig. S4). According to the XRD data, the average size of our electrocatalyst appears to be smaller at each metal loading than that of commercial one, consistent with our TEM results as shown in Fig. 2.

Furthermore, the phase-transferrable metallic complexes have been extended to PdCl_4^{2-} , AuCl_4^- , FeCl_6^{3-} , and CoCl_4^{2-} as shown in Figure S5. This makes this approach more general and allows us to easily manipulate the composition of electrocatalysts by combining above mentioned two or more metallic complexes at certain molar ratios. We have synthesized a variety of binary and ternary electrocatalysts, such as PtPd/C and PtPdAu/C. Figure S6 is the TEM image and EDX spectrum of PtPd/C, all PtPd nanostructures are well dispersed on carbon without free standing particles.

For applications, the surface of electrocatalysts is required to be clean and thus accessible for reactants, so CTAB molecules and other by-products need to be removed. We chose 59.9 wt% Pt/C to investigate the purification process and the electrochemical performance. The electrocatalyst was purified simply by washing with copious amount of water at 90-100 °C, different from the surfactant burning method that frequently causes size increase and shape modification.¹⁴ CV was used to detect the surface cleanness of the purified electrocatalyst. The initial 10 consecutive CV curves of Pt/C were recorded at 25 °C in N_2 -purged 0.1 M HClO_4 aq. with a scan rate of 100 mVs^{-1} by using a thin-film glassy carbon RDE. Figure S7a shows that

hydrogen adsorption and desorption peak of 59.9 wt% Pt/C appeared in the first cycle and remained unchanged during the following cycles. This suggests that the surface of the electrocatalyst is clean. Otherwise, the hydrogen adsorption/desorption peak will not appear initially or the peak would evolve with the removal of species covered on the surface by electrochemical oxidation. For comparison, CV curves (Figure S7b) were also collected for commercial 60 wt% Pt/C. Similar to 59.9 wt% Pt/C, hydrogen adsorption/desorption peak was observed right at the beginning of the CV test and did not change during the whole process. This indicates that our purified 59.9 wt% Pt/C is as clean as that of commercial 60 wt% Pt/C.

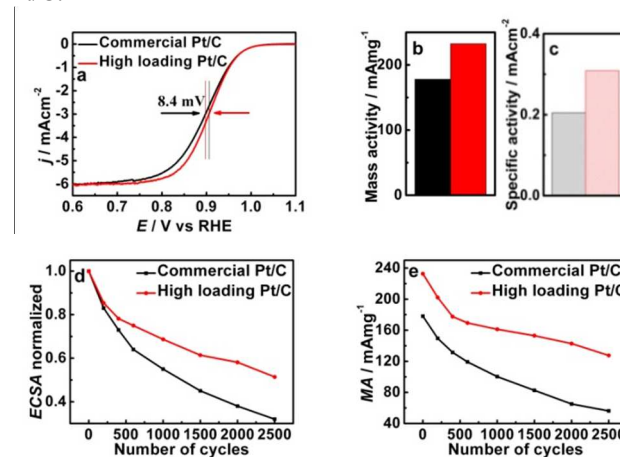


Figure 3. (a): ORR polarization curves measured in O_2 -saturated 0.1 M HClO_4 with a positive sweep rate of 10 mVs^{-1} at 1600 rpm (25 °C), (b) MA at 0.9 V (vs RHE), and (c) SA at 0.9 V (vs RHE) for 59.9 wt% Pt/C (red line) and commercial 60 wt% Pt/C (black line)), and their corresponding normalized ECSA values (d), and their corresponding MA values (e) recorded during the process of potential cycling (0.6-1.2 V vs. RHE, 100 mVs^{-1} , 0.1 M O_2 -purged HClO_4)

Figure 3a shows ORR polarization curves of 59.9 wt% Pt/C and commercial 60 wt% Pt/C obtained at 25 °C in O_2 -saturated HClO_4 (0.1 M) by using a thin-film glassy carbon RDE at 1600 rpm. The half-wave potential ($E_{1/2}$) of 59.9 wt% Pt/C is 8.4 mV more positive than that of commercial 60 wt% Pt/C. This suggests that our Pt/C is much more electro-catalytically active than commercial 60 wt% Pt/C. The mass activity (MA) of 59.9 wt% Pt/C is $232.7 \text{ mA mg}^{-1}_{\text{Pt}}$ at 0.9 V (vs. RHE), which is 1.31 times that of commercial 60 wt% Pt/C ($178.1 \text{ mA mg}^{-1}_{\text{Pt}}$) (Figure 3b), and the specific activity (SA) for 59.9 wt% Pt/C is $308.6 \text{ mA cm}^{-2}_{\text{Pt}}$, which is 51% higher than that of commercial 60 wt% Pt/C ($204.9 \text{ mA cm}^{-2}_{\text{Pt}}$) (Figure 3c). The much enhanced MA and SA of our Pt/C can be attributed to the small average size of 3.6 nm and the relative narrow size distribution of 20.4%. It is well known that 2-4 nm platinum nanoparticles possess the highest ORR activity when considering both ECSA and SA.¹⁵ Unlike commercial Pt/C (an average size of 4.4 nm with a wider size distribution of 29.9%), there are more platinum nanoparticles for our Pt/C falling in the optimum size range, thus leading to the much enhanced ORR activity.

Durability is also of special importance for practical applications.¹⁶ ADT over 59.9 wt% Pt/C and commercial 60 wt% Pt/C were performed by potential cycling between 0.6 and 1.2 V (vs. RHE) at a sweep rate of 100 mVs⁻¹ in O₂-purged HClO₄ solution (0.1 M). As shown in Figure S8, the CV curve of our Pt/C and commercial Pt/C shrinks with increased potential cycles. After ADT test, the ECSA loss of Pt/C is 48.6%, which is lower than that of commercial one (68.1%) (Figure 3d). The ORR curve of both electrocatalysts shift negatively during the ADT test. Interestingly, the degradation rate of our Pt/C is much slower than that of commercial one as shown in Figure 3e. After the ADT test, the MA value of our Pt/C (127.6 mAmmg⁻¹Pt) is 2.27 times of that of commercial Pt/C (56.2 mAmmg⁻¹Pt).

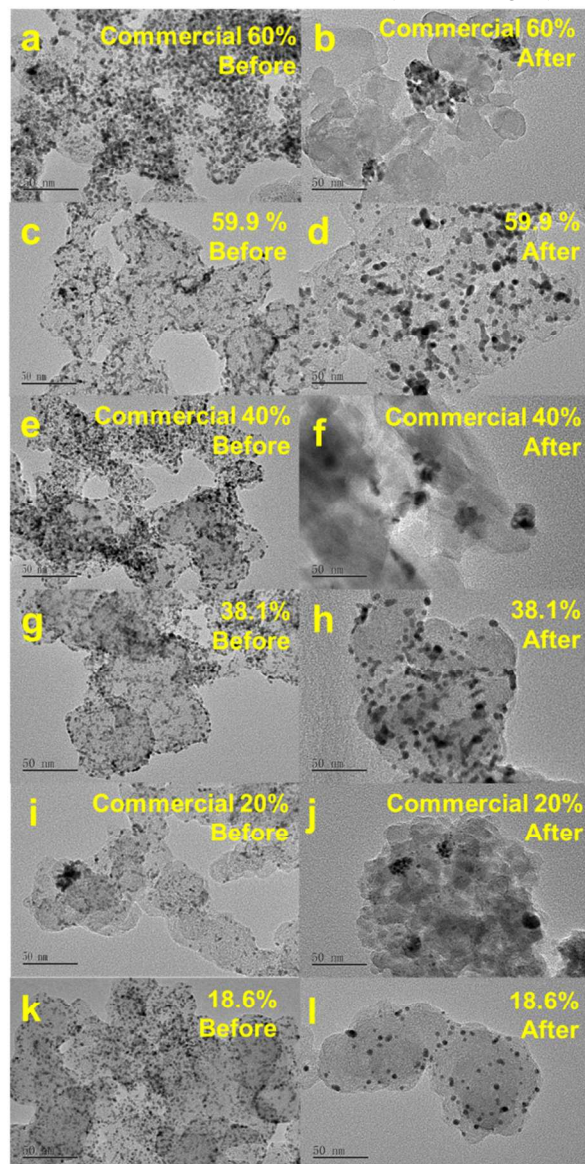


Figure 4. TEM images of 60 wt% commercial Pt/C, 59.9 wt% Pt/C, 40 wt% commercial Pt/C, 38.1 wt% Pt/C, 20 wt% commercial Pt/C and 18.6 wt% Pt/C before (a, c, e, g, i, k) and after (b, d, f, h, j, l) accelerated durability test. (0.6-1.2 V vs. RHE, 100 mVs⁻¹, 0.1 M O₂-purged HClO₄)

In order to elucidate the origin of the improved durability, we investigated the morphological changes by TEM before and after ADT (Figure 4a-d). The size of Pt nanoparticles of commercial Pt/C increased from 4-5 nm to 30-60 nm, because of the Pt dissolution-redeposition Ostwald ripening.¹⁷ In contrast, the size alteration of our Pt/C is a lot smaller after ADT (3-4 nm to 10-15 nm) likely related to the narrower size distribution, inherently resistant to Ostwald ripening which drives small nanoparticles gradually to become smaller and large ones to become larger via platinum dissolution and redeposition process. Similarly, 18.6 and 38.1 wt% Pt/C also show an improved durability compared with 20 and 40 wt% commercial Pt/C (Figure S9) owing to the narrow size distribution resistant to Ostwald ripening. The size changes of platinum nanoparticles of 18.6 and 38.1 wt% Pt/C during ADT is also smaller than that of corresponding commercial ones (Figure 4e-l).

Conclusion

In conclusion, we have demonstrated a controllable synthetic approach for the creation of platinum based electrocatalysts, especially at a high metal loading, by using metallic ion-containing reversed micelles adsorbed on carbon. This unique approach enables concurrent easy control over the size, size uniformity, metal loading, and composition of electrocatalysts, resulting in much improved ORR activity and durability. This controlled approach combined with facile surfactant removal method offers a general and effective avenue for producing next-generation of high-performance electrocatalysts.

Acknowledgements

This work was supported by National Key Basic Research Program of China (973 project, no. 2012CB215500), National Natural Science Foundation of China (project No.21306188, 21103163, 21373211, 21306187, and 21003114).

Notes and references

^a Dalian National Laboratories for Clean Energy (DNL), Dalian Institute of Chemical Physics (DICP), Chinese Academy of Sciences, 457 Zhongshan Road, Dalian 116023, P. R. China. Fax: 8641184379170; Tel: 8641184379831; E-mail: yjsong@dicp.ac.cn

^b Division of Chemical, Environmental and Biological Science and Technology, Dalian University of Technology, Dalian 116024, P. R. China.

† Electronic Supplementary Information (ESI) available: See DOI: 10.1039/b000000x/

1. J. Tollefson, *Nature*, 2010, **464**, 1262-1264.
2. (a) S. Guo, S. Zhang and S. Sun, *Angew. Chem., Int. Ed.*, 2013, **52**, 8526-8544; (b) M. K. Debe, *Nature*, 2012, **486**, 43-51; (c) J. Wu and H. Yang, *Acc. Chem. Res.*, 2013, **46**, 1848-1857; (d) C. Z. Zhu and S. J. Dong, *Nanoscale*, 2013, **5**, 10765-10775; (e) D. F. van der Vliet, C. Wang, D. Tripkovic, D. Strmcnik, X. F. Zhang, M. K. Debe, R. T.

- Atanasoski, N. M. Markovic and V. R. Stamenkovic, *Nat. Mater.*, 2012, **11**, 1051-1058.
3. (a) H. T. Chung, J. H. Won and P. Zelenay, *Nat Commun*, 2013, **4**, 1922; (b) G. Wu, K. L. More, C. M. Johnston and P. Zelenay, *Science*, 2011, **332**, 443-447; (c) Y. Li, W. Zhou, H. Wang, L. Xie, Y. Liang, F. Wei, J.-C. Idrobo, S. J. Pennycook and H. Dai, *Nat Nano*, 2012, **7**, 394-400; (d) Q. Wang, Z.-Y. Zhou, Y.-J. Lai, Y. You, J.-G. Liu, X.-L. Wu, E. Terefe, C. Chen, L. Song, M. Rauf, N. Tian and S.-G. Sun, *J. Am. Chem. Soc.*, 2014, **136**, 10882-10885; (e) C. W. Tsai, M. H. Tu, C. J. Chen, T. F. Hung, R. S. Liu, W. R. Liu, M. Y. Lo, Y. M. Peng, L. Zhang, J. J. Zhang, D. S. Shy and X. K. Xing, *RSC Adv.*, 2011, **1**, 1349-1357; (f) Z. H. Xiang, Y. H. Xue, D. P. Cao, L. Huang, J. F. Chen and L. M. Dai, *Angew. Chem., Int. Ed.*, 2014, **53**, 2433-2437; (g) Y. Xie, H. Li, C. Tang, S. Li, J. Li, Y. Lv, X. Wei and Y. Song, *J. Mater. Chem. A*, 2014, **2**, 1631-1635.
4. (a) C. Chen, Y. Kang, Z. Huo, Z. Zhu, W. Huang, H. L. Xin, J. D. Snyder, D. Li, J. A. Herron, M. Mavrikakis, M. Chi, K. L. More, Y. Li, N. M. Markovic, G. A. Somorjai, P. Yang and V. R. Stamenkovic, *Science*, 2014, **343**, 1339-1343; (b) C. Cui, L. Gan, M. Heggen, S. Rudi and P. Strasser, *Nat. Mater.*, 2013, **12**, 765-771; (c) H. Meng, F. Y. Xie, J. Chen, S. H. Sun and P. K. Shen, *Nanoscale*, 2011, **3**, 5041-5048; (d) K. Mohanraju and L. Cindrella, *RSC Adv.*, 2014, **4**, 11939-11947; (e) B. Y. Xia, H. B. Wu, Y. Yan, X. W. Lou and X. Wang, *J. Am. Chem. Soc.*, 2013, **135**, 9480-9485; (f) S. Li, H. Li, Y. Zhang, Robert M. Garcia, J. Li, Y. Xie, J. Yin, M. Li, J. Wang, J. A. Shelnett, T. Zhang and Y. Song, *J. Mater. Chem. A*, 2014, DOI: 10.1039/c3ta10406k.; (g) W. Si, J. Li, H. Li, S. Li, J. Yin, H. Xu, X. Guo, T. Zhang and Y. Song, *Nano Research*, 2013, **6**, 720-725.
5. D. Wang, H. L. Xin, R. Hovden, H. Wang, Y. Yu, D. A. Muller, F. J. DiSalvo and H. D. Abruña, *Nat. Mater.*, 2013, **12**, 81-87.
6. (a) S.-I. Choi, S. Xie, M. Shao, J. H. Odell, N. Lu, H.-C. Peng, L. Protsailo, S. Guerrero, J. Park, X. Xia, J. Wang, M. J. Kim and Y. Xia, *Nano Lett.*, 2013, **13**, 3420-3425; (b) V. D. Noto, E. Negro, S. Polizzi, F. Agresti and G. A. Giffin, *ChemSusChem*, 2012, **5**, 2451-2459
7. G. R. Zhang and B. Q. Xu, *Nanoscale*, 2010, **2**, 2798-2804.
8. (a) B. Y. Xia, W. T. Ng, H. B. Wu, X. Wang and X. W. Lou, *Angew. Chem., Int. Ed.*, 2012, **51**, 7213-7216; (b) Y. Kim, J. W. Hong, Y. W. Lee, M. Kim, D. Kim, W. S. Yun and S. W. Han, *Angew. Chem., Int. Ed.*, 2010, **49**, 10197-10201; (c) J. Greeley, I. E. L. Stephens, A. S. Bondarenko, T. P. Johansson, H. A. Hansen, T. F. Jaramillo, J. Rossmeisl, I. Chorkendorff and J. K. Nørskov, *Nat Chem*, 2009, **1**, 552-556; (d) B. Lim, M. Jiang, P. H. C. Camargo, E. C. Cho, J. Tao, X. Lu, Y. Zhu and Y. Xia, *Science*, 2009, **324**, 1302-1305; (e) L. Wang and Y. Yamauchi, *J. Am. Chem. Soc.*, 2013, **135**, 16762-16765; (f) L. L. Zou, J. Li, T. Yuan, Y. Zhou, X. M. Li and H. Yang, *Nanoscale*, 2014, **6**, 10686-10692; (g) W. Du, G. Yang, E. Wong, N. A. Deskins, A. I. Frenkel, D. Su and X. Teng, *J. Am. Chem. Soc.*, 2014, **136**, 10862-10865.
9. J. Ramousse, J. Deseure, O. Lottin, S. Didierjean and D. Maillet, *J. Power Sources*, 2005, **145**, 416-427.
10. (a) B. Fang, M.-S. Kim, J. H. Kim, M. Y. Song, Y.-J. Wang, H. Wang, D. P. Wilkinson and J.-S. Yu, *J. Mater. Chem.*, 2011, **21**, 8066-8073; (b) Z. Tian, F. Xie and P. Shen, *J. Mater. Sci.*, 2004, **39**, 1507-1509.
11. S. Rojas, F. J. Garcia-Garcia, S. Jaras, M. V. Martinez-Huerta, J. L. Garcia-Fierro and M. Boutonnet, *Appl. Catal. A- Gen.*, 2005, **285**, 24-35.
12. (a) P. Parthasarathy and A. V. Virkar, *J. Power. Sources*, 2013, **234**, 82-90; (b) B. C. Du and Y. Y. Tong, *J. Phys. Chem. B.*, 2005, **109**, 17775-17780
13. Y. Song, R. M. Garcia, R. M. Dorin, H. Wang, Y. Qiu, E. N. Coker, W. A. Steen, J. E. Miller and J. A. Shelnett, *Nano Lett.*, 2007, **7**, 3650-3655.
14. H. Yin, C. Wang, H. Zhu, S. H. Overbury, S. Sun and S. Dai, *Chem. Commun.*, 2008, 4357-4359.
15. K. Yamamoto, T. Imaoka, W.-J. Chun, O. Enoki, H. Katoh, M. Takenaga and A. Sonoi, *Nat Chem*, 2009, **1**, 397-402.
16. H.-H. Wang, Z.-Y. Zhou, Q. Yuan, N. Tian and S.-G. Sun, *Chem. Commun.*, 2011, **47**, 3407-3409.
17. R. Ouyang, J.-X. Liu and W.-X. Li, *J. Am. Chem. Soc.*, 2012, **135**, 1760-1771.